TASI-600 high resolution airborne thermal data for accurate materials detection in urban scenarios

Simone Pascucci[1], Angelo Palombo[1], Maria Daraio[1], Stefano Pignatti[1], Federico Santini[1] and Giovanni Laneve[2]

[1] *CNR IMAA, C.da S. Loja, 85050 Tito, Italy; simone.pascucci@imaa.cnr.it*
[2] *University of Rome La Sapienza - DIAEE, Rome, Italy; laneve@psm.uniroma1.it*

Abstract. The needs of useful tools for detecting and monitoring complex urban environments could benefit of new high spatial and spectral resolution thermal remote sensing data. In this sense and to face the most challenging future research themes in EO systems, the CNR IMAA has been upgraded its observing facilities, already composed by in situ hyperspectral and IR broadband sensors, airborne VSWIR hyperspectral sensors and multi-mission satellite receiving stations, with the TASI-600 hyperspectral scanner. The TASI-600 sensor has 32 bands in the LWIR (8.0-11.5 μm) spectral range, with a swath of 600 pixels for a FOV of 40° and an IFOV of 1.2 mrad. This study deals with TASI-600 airborne thermal data preprocessing carried out as follows: (a) radiometric calibration of the raw data and blinking pixels correction; (b) atmospheric correction of the TIR data; (c) separation of temperature and emissivity. Once retrieved emissivities for the complex urban scenario of the proposed study area located in Southern Italy, spectral classification algorithms have been tested and applied in order to retrieve and accurately classify surface materials occurring in this complex site. The paper presents the results of TASI-600 acquisition over this test site highlighting that the high spectral and radiometric resolution enables the accurate mapping of a range of surface materials, thus allowing for a preliminary characterization of urban materials and being an effective means to quantitatively monitor urban materials status and their possible alteration.

Keywords. TASI-600; Hyperspectral thermal data; Emissivity; Urban materials.

1. Introduction

Hyperspectral remote sensing research studies over the last decades have set up a framework for image analysis and processing routines, field calibration and validation of data sets, and recognized the nominal wavelength range for surface mineral and material detection [1, 2]. Concerning the Thermal InfraRed (TIR) spectral range, it has been used for geologic studies to map surface minerals based on differences in spectral absorption features i.e. band centers and other spectral feature positions [3].

Infrared technology has been significantly improved, however, while visible and near-infrared (VNIR) and short wave infrared (SWIR) hyperspectral data have been applied for more than a decade for urban applications [2, 4], there are currently a limited number of multi/hyperspectral thermal instruments that operate in the long-wavelength infrared (LWIR) spectral region (8-12 μm). Among them, SEBASS [3] that measures the MWIR/LWIR spectral ranges; TASI-600 (Thermal Airborne Spectrographic Imager) operating in the LWIR [5], SPECIM AisaOWL and HyTES (recently developed by NASA JPL) airborne sensors. Moreover, in the same LWIR interval also interferometer technologies such as TELOPS FIRST are at present operating, while the ONERA SYSIPHE sensors will be available in the next years.

These new technologies require new methods to assess an appropriate pre-processing chain in order to provide consistent products to be used for different applications such as soil, urban and environmental applications. Thermal detectors are, in fact, characterized by artifacts that are less evi-

dent in other kind of sensors, such as anomalous pixels, i.e. dark, saturated and blinking pixels that are typical of thermal detectors. In this context, for accurate materials detection in urban scenarios, even if satellite data have provided considerable improvements in our knowledge of urban surface properties, improvements in radiometric, spatial and temporal characteristics are still needed for urban studies [6]. Because of the lack of suitable satellite based hyperspectral sensors for urban areas, most studies have been carried out with airborne multi/hyperspectral sensors. Different methods and additional data were applied to VNIR-SWIR hyperspectral data in the last decade by using different spectral analysis techniques to characterize man made materials [2, 4, 6].

In this paper, we describe the utility of TASI-600 high resolution airborne thermal data for accurate materials detection in urban scenarios using airborne dataset acquired over a flat urban area in southern Italy. TASI-600 imagery was pre-processed and used to assess its utility for urban material studies by mapping surface emissivities properties at 1 m spatial resolution.

2. Methods

2.1. TASI-600 data and preprocessing

The TASI-600 is a pushbroom hyperspectral sensor operating in the LWIR (8-11.5 μm) spectral region [7] with 32 bands and a swath of 600 pixels for a Field Of View (FOV) of 40° and an IFOV of 1.13 mrad. The TASI-600 system is composed by the Scan Head Unit (SHU) provided with a custom Stirling Cycle cooled MCT detector (HgCdTe) and the Instrument Control Unit (ICU) and also of licensed pre-processing software to radiometrically (RADCORR) and geometrically (GEOCOR) correct TASI-600 data. RADCORR removes system offsets (i.e. dark current) and data can be output as spectral mSRU radiance units (1 mSRU is equal to 1 nW cm-2 sr-2 nm-1) or apparent temperatures; while, the GEOCOR software incorporates photogrammetric bundle adjustment solutions to produce orthorectified images using precision IMU/GPS and terrain height data. The instrument was mounted on a Partenavia P68 Observer airborne and the presented data were acquired on June 16, 2011 between 10:50 and 12:50 (GMT) during a TASI-600 campaign conducted on Pontecagnano (Italy), a flat urban area with different urban land cover and surface materials. The study area corresponds to six TASI-600 stripes with an overlapping area of 60% and 80% for the horizontal and vertical images, respectively (Figure 1) acquired using an integration time of 0.32 ms, at an altitude of 850 m corresponding to a ~1.0 m ground pixel resolution at the instrument's IFOV. This area was also used to perform the parameter assessment used for the geometric correction (i.e. the bundle adjustment).

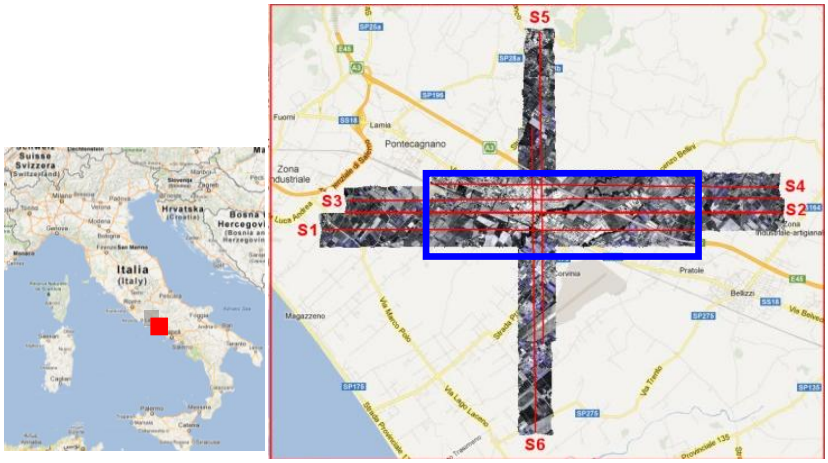

Figure 1. The six TASI-600 stripes overlaid on Google Maps showing the location of the study area (blue box).

TASI-600 radiometric correction of the data was performed both by using the RADCORR software provided by ITRES (Canada) and by applying a new correction tool for blinking pixel correction, developed by CNR IMAA (Italy) to refine the radiometric accuracy and to apply a new procedure to solve the blinking pixels correction problem affecting thermal MCT sensors. TASI radiance images were orthorectified by using the GEOCORR software obtaining an accuracy of 2 pixels (i.e. 2 m).

The atmospheric correction of the orthorectified radiances was performed by applying the ISAC (In-Scene Atmospheric Compensation) algorithm [7]. This algorithm is commonly used for in scene atmospheric thermal data correction when the atmospheric radiative conditions are not available during the acquisition time. It assumes two pixels of the scene to be blackbodies of which neither locations nor temperatures are known. For this study, we have applied the "All – Normalized Regression" method as described by [7], by estimating the surface temperature for each pixel using the maximum value of the brightness temperatures found throughout the input wavelengths. After the atmospheric compensation, the "emissivity normalization routine" [8] was applied to separate temperature and emissivity (TES). This routine derives first the brightness temperature of each pixel from the pixel radiance. Then, the apparent emissivity image is obtained by normalizing the radiance of each pixel to the Planck's curve that is generated from the pixel with the maximum brightness temperature with an emissivity value set to 0.98 (reasonable hypothesis for this study area).

2.2. Classification methods

Input spectra for both the classification methods used were derived from Regions of Interest (ROI), not acquired during field campaigns, drawn directly on the emissivity images (Figure 2). Figure 2 shows the mean TASI-600 emissivity spectra of the classes used for the applied classification methods. We randomly split the validation dataset into two parts that we use as training and validation dataset, respectively, in order to evaluate the accuracy of the classification methods and robustness with respect to the training dataset. The land cover classes used for this study to retrieve the land cover capability mapping of the TASI-600 emissivities are resumed in Table 1, with the number of pixels used for training and validation purposes. The paving materials were trained using the spectra pertaining to the asphalt (new and old) and cement; the roofing materials were trained using the red, grey and ceramic tiles, metal sheets, greenhouse plastic, cement spectra; the vegetation class was trained with grass and trees; the soil class was trained with different soil types (red, dark, and brownish soils) and abandoned greenhouses with bare soil outcropping (Table 1).

Classification of TASI-600 emissivity imagery aimed at discriminating different urban land cover types using multivariate information coming from several spectral bands to classify surface materials occurring in this complex urban site. To this aim two commonly used supervised classification method as Spectral Angle Mapper (SAM) [9] and Support Vector Machine (SVM) [10] were applied for the selected ROI. The SAM algorithm allows performing a quick test on the spectral orthogonality of the urban material spectral classes by determining the spectral similarity between two spectra through the calculation of the angle between the spectra and treating them as vectors in a space with dimensionality equal to the number of bands. The SVM is a supervised classifier derived from statistical learning theory and successfully applied for hyperspectral data providing accurate results in mapping complex decision boundaries such as urban land covers. It is a nonparametric, binary classifier functioning as a multiclass classifier separating the classes with a decision surface (optimal hyperplane) that maximizes the margin between the classes and the data points closest to the hyperplane ("support vectors").

Table 1. Land cover classes used for this study with the size of the training and validation datasets.

		Classes	Training pixels	Validation pixels
Rural	Veg.	vegetation trees	10612	5653
		grass	6989	5103
	Soil	red soil (a)	997	909
		red soil (b)	5320	4154
		brownish soil	5444	5222
		dark soil	3176	2604
		greenhouse (a)	2977	1658
Urban	Paving	old asphalt (a)	5630	3266
		old asphalt (b)	863	637
		new asphalt (a)	3566	2868
		new asphalt (b)	2794	2122
		cement pavement	155	59
	Roofing	metal roof (a)	5660	1052
		metal roof (b)	1028	992
		red tiles roof	1471	1422
		gray tail roof	1328	968
		red concrete roof	768	767
		cement roof	2594	962
		flat roof of ceramic tiles	269	158
		solar panel	482	682
		greenhouse (b)	5531	4938

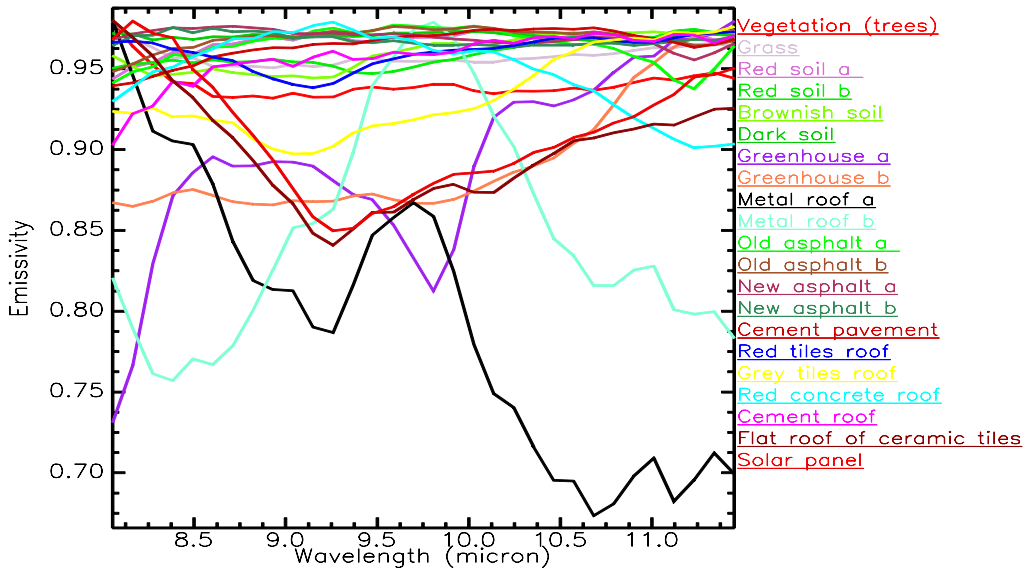

Figure 2. Mean TASI-600 emissivity spectra of the classes used for SAM and SVM classification.

3. Results

Figure 3 and Table 2 show the results of the SAM (Figure 3a) and SVM (Figure 3b) classification attained for the TASI-600 dataset. Both SAM and SVM results show that TASI-600 emissivities were able to discriminate different paving and roofing materials from soils and vegetation with a good accuracy. More in detail, in Figure 3 are presented the (a) SAM and (b) SVM classification results obtained for the analyzed 13 land cover classes.

In Table 2 are reported the confusion matrix obtained by using the selected validation ROIs. As reported in Table 2 the SVM classifier provided better results than the SAM classifier in discrimi-

nating the analyzed classes. Overall Accuracies obtained by the two classification methods are of 92.1479% and 81.9710% and Kappa Coefficients of 0.9040 and 0.7814, respectively.

As regards the roofing materials, both SAM and SVM classifiers achieved a good accuracy in discriminating the different classes with low percentage of errors except for the cement roofs that are almost spectrally confused with soil classes as highlighted in the confusion matrix presented in Table 2. The cement roof class is therefore not reliable as the spectral signature of this material is characterized by an emissivity behavior with the lack of peculiar spectral features that strongly affects its spectral separability from the emissivity shape of soil classes, i.e. their detection.

Moreover, SAM classification produced low accuracies in classifying the asphalt new (38.1% classified as greenhouse) and asphalt old (22.1% classified as soil and 23.7% cement pavement) classes. This is almost due the fact that the spectral signature of this material is characterized by a low emissivity (i.e. low SNR) and the lack of peculiar spectral features affects its detectability as this classifier determines the spectral similarity between the input spectra through the calculation of the angle between the spectra. Whereas, SVM classification results are more consistent and with a high accuracy level, the only class with significant errors is the cement material both used for roofing (57.9% classified as soil) and paving (15.3% classified as asphalt old).

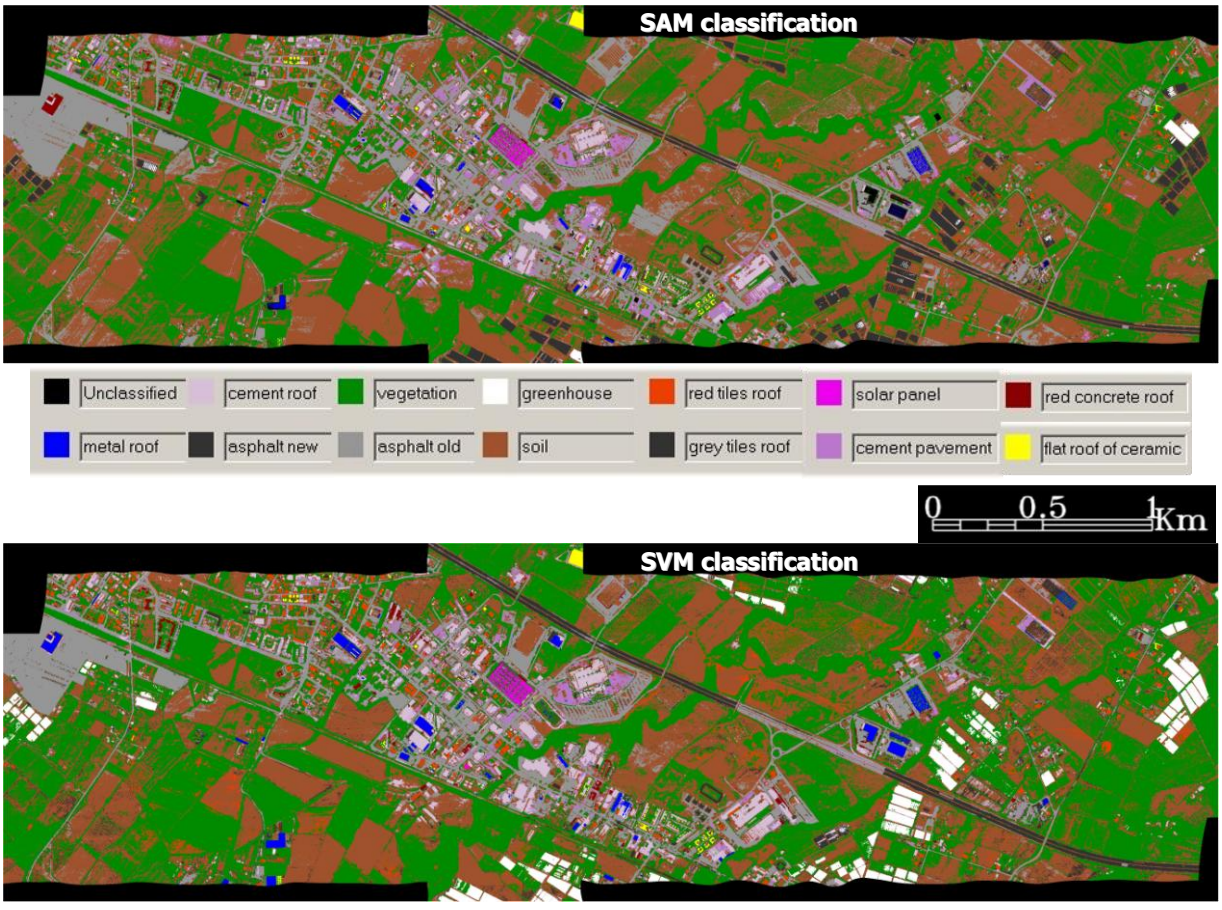

Figure 3. (a) SAM and (b) SVM classification results.

Table 2. Performance indicators for the SAM (a) and SVM (b) methods applied to the TASI-600 emissivities: Overall Accuracy, K coefficient.

SAM

	metal roof	vegetation	asphalt old	red tiles roof	grey tiles roof	red concrete roof	cement roof	asphalt new	greenhouse	soil	solar panel	cement pavement	flat roof of ceramic tiles	Total
Unclassified	1.4	0.0	0.0	0.0	0.0	0.0	0.0	0.0	0.0	0.0	0.0	0.0	0.0	0.1
metal roof	91.7	0.0	0.0	0.0	0.0	0.0	0.0	0.0	0.0	0.0	0.0	0.0	0.0	3.5
vegetation	0.2	98.9	0.0	0.1	0.0	0.0	0.0	0.8	0.0	0.5	1.7	0.0	0.6	29.0
asphalt old	3.9	0.0	100.0	0.0	0.0	4.0	6.8	2.4	0.0	22.1	0.0	23.7	0.0	13.8
red tiles roof	0.0	0.1	0.0	97.3	0.0	0.0	6.5	0.0	0.0	0.1	0.0	0.0	0.0	2.9
grey tiles roof	0.0	0.0	0.0	0.1	98.6	0.0	7.4	0.0	13.4	0.0	0.0	0.0	0.0	4.6
red concrete roof	1.0	0.0	0.0	0.0	0.0	94.0	0.0	0.0	0.0	0.0	0.0	0.0	0.0	1.4
cement roof	0.0	0.0	0.0	0.0	0.1	0.0	6.7	0.0	0.0	1.0	0.0	0.0	0.0	0.6
asphalt new	0.3	0.0	0.0	0.0	0.0	1.0	0.0	57.4	0.0	0.0	0.0	0.0	0.0	5.3
greenhouse	0.0	0.0	0.0	0.0	0.0	0.0	0.0	38.1	85.6	0.0	0.2	0.0	0.0	14.9
soil	0.3	1.0	0.0	2.5	1.4	0.9	65.8	1.3	1.1	72.0	0.0	8.5	0.0	21.3
solar panel	0.0	0.0	0.0	0.0	0.0	0.0	0.0	0.0	0.0	0.0	97.5	0.0	0.0	0.9
cement pavement	1.2	0.0	0.0	0.0	0.0	0.0	6.8	0.0	0.0	4.5	0.0	67.8	0.0	1.5
flat roof of ceramic tiles	0.0	0.0	0.0	0.0	0.0	0.0	0.0	0.0	0.0	0.0	0.6	0.0	99.4	0.3
Total	100.0	100.0	100.0	100.0	100.0	100.0	100.0	100.0	100.0	100.0	100.0	100.0	100.0	100.0

(a)

SVM

	metal roof	vegetation	asphalt old	red tiles roof	grey tiles roof	red concrete roof	cement roof	asphalt new	greenhouse	soil	solar panel	cement pavement	flat roof of ceramic tiles	Total
Unclassified	0.0	0.0	0.0	0.0	0.0	0.0	0.0	0.0	0.0	0.0	0.0	0.0	0.0	0.0
metal roof	91.5	0.0	0.0	0.0	0.0	0.0	0.0	0.0	0.0	0.0	0.0	0.0	0.0	3.5
vegetation	3.7	100.0	0.0	0.0	0.1	1.6	0.0	0.8	0.0	1.3	1.5	0.0	0.0	29.6
asphalt old	0.2	0.0	97.9	0.0	0.0	0.4	7.1	0.5	0.0	7.4	0.0	15.3	0.0	9.7
red tiles roof	0.0	0.0	0.0	98.7	0.1	0.0	8.1	0.0	0.0	0.5	0.4	0.0	0.0	3.1
grey tiles roof	0.0	0.0	0.0	0.1	98.0	0.0	0.7	0.0	0.0	0.0	0.0	0.0	0.0	2.5
red concrete roof	0.6	0.0	0.2	0.0	0.0	97.1	0.0	0.0	0.0	0.0	0.0	0.0	0.0	1.4
cement roof	0.2	0.0	0.0	0.0	1.2	0.0	24.1	0.0	0.0	3.9	0.0	0.0	0.0	2.1
asphalt new	0.0	0.0	1.5	0.0	0.0	0.0	0.1	98.4	0.0	0.2	0.0	0.0	0.0	9.3
greenhouse	3.6	0.0	0.0	0.0	0.1	0.0	0.0	0.0	99.9	0.0	0.0	0.0	0.0	13.4
soil	0.1	0.0	0.3	1.1	0.6	0.9	57.9	0.2	0.1	86.1	0.0	13.6	0.0	23.8
solar panel	0.0	0.0	0.0	0.0	0.0	0.0	0.0	0.0	0.0	0.0	98.1	0.0	0.0	0.9
cement pavement	0.0	0.0	0.1	0.0	0.0	0.0	2.0	0.0	0.0	0.7	0.0	71.2	0.0	0.4
flat roof of ceramic tiles	0.0	0.0	0.0	0.0	0.0	0.0	0.0	0.1	0.0	0.0	0.0	0.0	100.0	0.3
Total	100	100	100	100	100	100	100	100	100	100	100	100	100	100

(b)

4. Conclusions

The TASI-600 is an advanced and suitable thermal hyperspectral sensor, with optimal radiometric performances and high spectral resolution, this makes the sensor valuable to the science community involved in the Earth's environment and in particular for urban studies in applications devoted to land cover mapping and monitoring, materials identification, heat islands measuring and mapping, etc.

Although it is challenging to measure ground surface emissivity because of the difficulties of atmospheric correction and temperature/emissivity separation, we believe that using emissivity could allow a better exploitation of TASI TIR hyperspectral data by anabling an accurate detection of the absorption features of a range of TIR-active minerals (e.g., alunite, asbestos, carbonate rocks, gypsum, kaolinite/halloysite, and montmorillonite/illite) and materials (asphalts, cement, plastic, metals, etc.).

Future applications will be focused on fusion algorithms development (VIS & TIR spectra + TIR spectroscopy and thermal imaging) by evaluating the impact of the 60 m spatial resolution on those objectives and synergies in view of the urban remote sensing opportunities offered by the future HyspIRI satellite mission.

Acknowledgements

We would like to thank an anonymous reviewer, whose thoughtful comments helped to improve the final manuscript.

References

[1] Clark, R. N., 1999. *Spectroscopy of rocks and minerals and principles of spectroscopy*. In A. N. Rencz (Ed.), Remote sensing for the Earth sciences (3rd Ed). Manual of Remote Sensing, vol. 3. (pp. 3–52) NY: John Wiley & Sons, Inc.

[2] Heiden, U., Segl, K., Roessner, S., & Kaufmann, H., 2007. *Determination of robust spectral features for identification of urban surface materials in hyperspectral remote sensing*. Remote Sensing of Environment, 111, 537–552.

[3] Vaughan, R. G., Hook, S. J., Calvin,W. M., & Taranik, J. V., 2005. *Surface mineral mapping at Steamboat Springs, Nevada, USA, with multi-wavelength thermal infrared images*. Remote Sensing of Environment, 99(1–2), 140–158.

[4] Pascucci, S., Bassani, C., Palombo, A., Poscolieri, M., & Cavalli, R., 2008. *Road asphalt pavements analyzed by airborne thermal remote sensing: Preliminary results of the Venice highway*. Sensors, 8 (2), pp. 1278-1296.

[5] Pignatti, S., Lapenna, V., Palombo, A., Pascucci, S., Pergola, N. & Cuomo, V. 2011. *An advanced tool of the CNR IMAA EO facilities: Overview of the TASI-600 hyperspectral thermal spectrometer*. Hyperspectral Image and Signal Processing: Evolution in Remote Sensing (WHISPERS), pg. 1-4. 3rd Workshop on Remote Sensing.

[6] Weng, Q., & Quattrochi, D. A., 2006. *Thermal remote sensing of urban areas: An introduction to the special issue. Remote Sensing of Environment*, 104, 119–122.

[7] Johnson, B. R. & Young, S. J., 1998. In-*Scene Atmospheric Compensation: Application to SEBASS Data Collected at the ARM Site.* Technical Report, Space and Environment Technology Center, The Aerospace Corporation, May 1998.

[8] Li, Z.L., Becker, F., Stoll, M.P. & Wan, Z., 1999. *Evaluation of six methods for extracting relative emissivity spectra from thermal infrared images.* Remote Sensing of Environment, vol. 69, 197-214.

[9] Chan, C.I. *Hyperspectral Imaging: Techniques for Spectral Detection and Classification*. Kluwer Academic Publishers, Dordrecht, 2003.

[10] Melgani, F. & Bruzzone, L., 2004. *Classification of Hyperspectral Remote Sensing Images with Support Vector Machines*. IEEE Transactions on Geoscience and Remote Sensing, Vol. 42, No. 8, August 2004.